Aleksandar Borković, University of Banja Luka, aleksandar.borkovic@aggf.unibl.org
Miloš Jočković, University of Belgrade, mjockovic@grf.bg.ac.rs
Dijana Tatar, University of Banja Luka, dijana.majstorovic@aggf.unibl.org
Snježana Milovanović, University of Banja Luka, snjezana.milovanovic@aggf.unibl.org

A NOTE ON BEAM-TO-BEAM CONTACT DYNAMICS

Abstract

Two approaches for beam-to-beam contact modeling are considered in the paper. The first is the classic continuum approach with point-to-point contact discretization. The other is the coarse-grained approach where the physical intermolecular fields are applied for the modeling of interaction of continuous bodies. To describe the contact, the repulsive steric potential is utilized here. The advantages and disadvantages of both approaches are discussed, and the results are compared with those obtained in Abaqus. An involved computational simulation of multiple collisions between elastic beams is considered as a numerical example.

Keywords: beam-to-beam contact dynamics; coarse-grained model; intermolecular forces

ЈЕДАН ОСВРТ НА ДИНАМИКУ КОНТАКТА ГРЕДА-ГРЕДА

Сажетак

У раду су размотрена два приступа моделирању контакта греда-греда. Први је приступ класичне механике континуума са дискретизацијом контакта на нивоу тачка-тачка. Други је модел грубе апроксимације код кога користимо физичка интермолекуларна поља да опишемо међудјеловање континуалних тијела. За описивање контакта, примијењен је одбојни стерични потенцијал. Размотрене су предности и мане оба приступа, те су добијени резултати упоређени са онима из Абакуса. Као нумерички примјер, размотрена је сложена рачунска симулација вишеструких судара између еластичних греда.

Кључне ријечи: динамика контакта греда-греда; модел грубе апроксимације; међумолекуларне силе

1. INTRODUCTION

Slender bodies are readily found in nature, nanotechnology, biomechanics, engineering, etc. Due to the well-known limitations of physical experiments, numerical simulations of systems involving slender bodies are of utmost importance. One of the most successful mechanical models is that of a beam. The mechanical beam model allows accurate and efficient simulations of real-life systems involving slender bodies. When a mechanical system consists of multiple beams undergoing large deformations, there is a possibility that the beams will interact with each other. From a macroscopic point of view, this interaction is often perceived as a *mechanical contact* caused by the impenetrability of the interacting bodies. However, on the micro- and nano- level, the interaction can be both attractive and repulsive, due to the effects of various intermolecular fields. These fields manifest themselves as intermolecular forces that are the gradients of interaction potentials between molecules/particles. Some well-known interaction potentials are gravitational, electrostatic, van der Waals, steric, etc.

The interaction between assemblies of molecules is readily modeled as a particle-particle interaction via *molecular dynamics* [1]. Within this approach, we apply the laws of motion on each particle, which results in an accurate, but computationally expensive simulation, Fig. 1a.
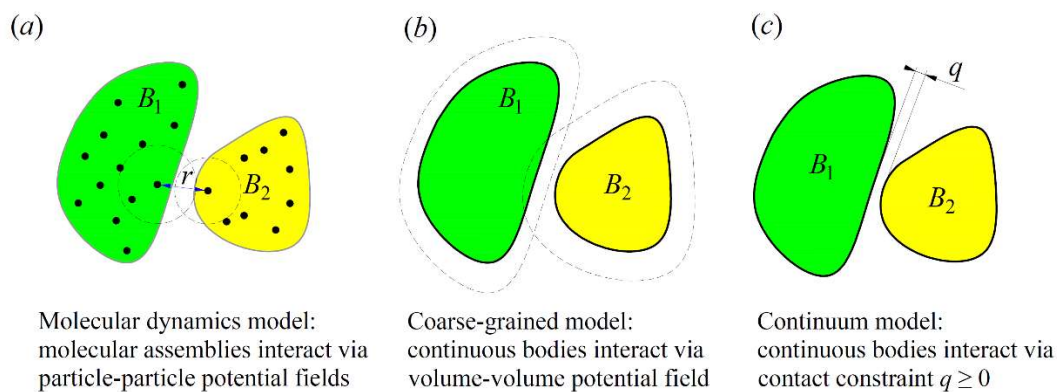

Figure 1. Contact interaction models. (adopted from [2])

On the other hand, the continuum contact approach considers the interaction between continuous bodies and imposes the contact conditions, e.g. impenetrability of interacting bodies, Fig. 1c. This approach is well-established and efficient [3], but lacks a rigorous physical foundation. A middle ground between these two approaches is the *coarse-grained* method, Fig. 1b, which combines the fundamental physics of intermolecular forces and the efficiency of the continuum mechanics [2].

In this paper, we consider one type of the penalty point-to-point method for the contact interaction between arbitrarily curved elastic beams. The interacting closest points are selected from a set of discrete integration points. The proposed formulation provides a straightforward description of contact, ensuring a simple implementation while preserving good accuracy. Additionally, we consider the coarse-grained method that is based on the homogenization of interaction potential and its pre-integration over the beam cross-sectional areas [4].

The NURBS basis functions are utilized for the spatial discretization of the Bernoulli-Euler beam model within the framework of the isogeometric analysis (IGA) [5]. For the time discretization, the well-known HHT implicit scheme is applied.

The paper is organized as follows. The main ingredients of the employed contact models are introduced in the next section. Then, the fundamental aspects of the Bernoulli-Euler beam theory and implicit time discretization are presented. Section 4 deals with the definition and properties of the NURBS functions, while the numerical experiment is discussed in Section 5. Conclusions and guidelines for future research are given in the last section.

2. CONTACT MECHANICS

The total potential energy, Π_{tot}, of a conservative mechanical system consists of the internal strain energy Π_{int}, the kinetic energy Π_{kin}, and the work of external forces Π_{ext}. If the bodies interact

with each other, the interaction contact energy, Π_{con}, must be taken into account as well. The weak form of equilibrium requires that the variation of the total potential energy with respect to the generalized coordinates is zero, i.e.

$$\delta\Pi_{tot} = \delta\Pi_{int} + \delta\Pi_{kin} + \delta\Pi_{ext} + \delta\Pi_{con} = 0. \tag{1}$$

The strain and kinetic energy are readily derived in the literature, and we will only briefly refer to them in Section 3. The work of external forces is not considered in this paper. Our focus is on the contact interaction potential. Two approaches for the definition of contact contribution Π_{con} are discussed in this section.

2.1. CONTINUUM APPROACH

Computational contact mechanics provides accurate and efficient numerical methods for the modeling of contact interaction between solid bodies [3]. A special case of the contact between solid bodies is the contact between beams. The beam-to-beam contact is a well-researched area [6], but many issues are yet to be tackled [7]. The existing continuum formulations for the beam-to-beam contact differ in various aspects of computational modeling, such as: the definition of contact condition, contact discretization, contact search, optimal integration strategy, etc. Some of the well-known approaches for enforcing the contact condition are the penalty method, the Lagrange multipliers, the augmented Lagrange method, etc. Regarding the contact discretization, there are point-to-point, point-to-segment, segment-to-segment approaches, and various variations.
In this paper, we focus on the penalty point-to-point beam contact formulation. Let us consider two arbitrarily curved beams with the cross-sectional radii R_1 and R_2, see Fig.1.
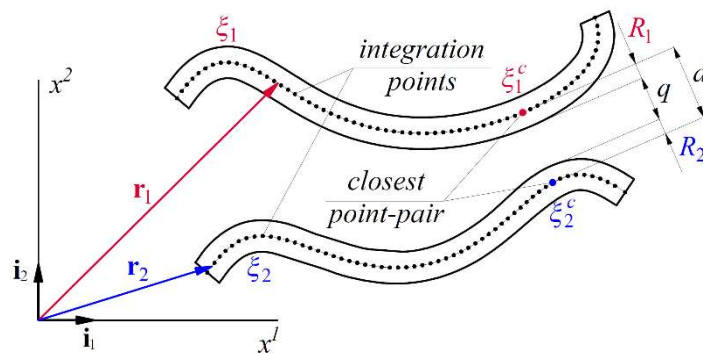

Figure 2. Interaction of two planar beams. Integration point-to-integration point contact discretization.

The beam centerlines are defined with curves $\mathbf{r}_1(\xi_1)$ and $\mathbf{r}_2(\xi_2)$. To determine the location of contact between the beams, it is necessary to identify the closest point positions where the prohibited penetration is enforced by the contact constraints. The closest point positions, ξ_1^c and ξ_2^c, can be found by minimizing the distance between beam axes, $d = \|\mathbf{r}_1 - \mathbf{r}_2\|$. The minimization requires that the tangents of both beams at the closest points are perpendicular to the distance vector $\mathbf{d} = \mathbf{r}_1 - \mathbf{r}_2$. This procedure leads to two nonlinear equations with unknown positions of closest points.
The non-penetration condition at the closest point-pair is formulated using an inequality constraint

$$q = d_{min} - R_1 - R_2 \geq 0, \tag{2}$$

where q is the gap function. This constraint allows us to define the contact interaction energy as

$$\Pi_{con} = \begin{cases} \dfrac{1}{2}\varepsilon q^2, & q \leq 0 \\ 0, & q > 0 \end{cases}, \tag{3}$$

where ε is the penalty parameter. The variation of the gap with respect to the configuration of a system gives

$$\delta q = \delta d_{min} = \delta[(\mathbf{r}_1 - \mathbf{r}_2) \cdot (\mathbf{r}_1 - \mathbf{r}_2)]^{1/2} = \hat{\mathbf{d}}(\delta \mathbf{r}_1 - \delta \mathbf{r}_2), \tag{4}$$

where $\hat{\mathbf{d}}$ is the unit distance vector that equals the normal vector for the closest point-pair. The variation of the contact potential results with the point contact contribution to the weak form, i.e.

$$\delta \Pi_{con} = \varepsilon \, \delta q = \varepsilon \, q \, \hat{\mathbf{d}}(\delta \mathbf{r}_1 - \delta \mathbf{r}_2) = \mathbf{f}_{con}\delta \mathbf{r}_1 - \mathbf{f}_{con}\delta \mathbf{r}_2, \tag{5}$$

where $\mathbf{f}_{con}$ is the contact force [7]. With this formulation, the contact interaction between two beams manifests as a discrete point force acting at the closest points of the beam centerlines along the normal direction.

One issue with the described point-to-point approach is that the closest point procedure does not have a guaranteed unique solution, e.g. when considering parallel beams. Another issue is that the contact traction is modeled as a point force, while we anticipate the distributed traction for the case of contact between nearly parallel beams. These issues can be tackled by specific procedures, such as the line-to-line contact discretization [7].

In this paper, we address the issue of the non-uniqueness of closest point-pairs by searching for the closest discrete point-pairs. We define a dense distribution of integration points, and search for the closest point-pairs between them, see Fig. 2. As the number of integration points increases, this approach converges to the previously described closest point algorithm. We refer to this approach as the integration point-to-integration point (IPIP) contact discretization. Importantly, this dense distribution of integration points is only used for the integration of the contact potential. The proposed approach stems as a special case of the algorithm used for the coarse-grained formulation which is discussed in the next subsection. Additionally, the bias of the standard master-slave approach can be avoided with the proposed discretization, but further investigation on this issue is required.

2.2. COARSE-GRAINED APPROACH

The idea behind the coarse-grained (CG) approach is to assume that the interaction potential between assemblies of molecules (interacting bodies) can be smeared over the volumes, allowing us to replace the summation with the integration. The method is well-established and applied in various scenarios for both long- and short-range interactions [2, 4, 8]. In this subsection, we give a brief introduction to the CG approach.

An interaction potential $\hat{\Phi}_m$ between two particles is usually assumed as an inverse-power law:

$$\hat{\Phi}_m = k_m r^{-m}, \tag{6}$$

where k_m is the physical constant, and r is the distance between the particles, see Fig. 1a. The usual assumption is that the total interaction potential between two bodies, B_1 and B_2, can be approximated as a pairwise summation of individual interactions, i.e.

$$\Phi_m = \sum_{I \in B_1} \sum_{I \in B_2} k_m r_{IJ}^{-m}, \tag{7}$$

where r_{IJ} is the distance between particles I and J. This expression corresponds to the molecular dynamics approach. By assuming that the interaction potential can be coarse-grained and homogenized over the interacting bodies, we can write

$$\Phi_m \approx \Pi_{con} = \int_{V_1} \int_{V_2} k_m \beta_1 \beta_2 r_m^{-m} dV_1 dV_2, \tag{8}$$

where β_i are the densities of interacting particles. This expression represents the basis of the CG approach, see Fig. 1b.

The calculation of two nested 3D integrals in (8) is complicated and several simplifications have been introduced for specific applications [8]. For the beam-to-beam interaction, a so-called *section-section interaction potential* approach is introduced in [4]. By pre-integrating the interaction potential over the cross sections, the integral (8) reduces to 2D, i.e.

$$\Phi_m = k_m \beta_1 \beta_2 2^{5/2-m} \pi^{3/2} \sqrt{\frac{R_1 R_2}{R_1 + R_2}} \frac{\Gamma(m-7/2)}{\Gamma(m/2)^2} \int_{L_1} \int_{L_2} q^{-m+7/2} ds_2 ds_1, \tag{9}$$

where $\Gamma(z)$ is the Gamma function. The expression (9) is only approximate since it disregards the offset between cross sections [9]. However, it is arguably well-suited for contact modeling based on the steric repulsion field with $m = 12$.

Many issues need to be addressed for the successful implementation of the CG approach, such as the regularization of the potential law, accuracy of the section-section interaction, efficient integration, etc. Let us discuss one important feature - the cutoff distance. Since the interaction potentials are defined as the inverse-power laws with respect to the distance, it is practical to consider some cutoff value. For this, we define the cutoff distance as the radius of a circle around the particle, outside of which the effect of the interaction force is neglected. It allows us to reduce the number of interacting point-pairs and to keep only the important contributions. If the short-range interactions are considered ($m > 3$), the introduction of the cutoff distance can improve the efficiency without significantly affecting the accuracy.

The main advantages of the CG approach are: (i) it is based on the fundamental intermolecular laws and (ii) it models contact as distributed traction. The main disadvantages are: (i) accurate pre-integration is difficult and often impossible and (ii) the integration is more involved, in comparison with the IPIP approach, since more points interact with each other.

3. IMPLICIT DYNAMIC ANALYSIS OF BERNOULLI-EULER BEAM

According to the Bernoulli-Euler (BE) hypothesis that a beam's cross section is rigid and perpendicular to the beam axis in all configurations, a 3D continuum model of the planar beam degenerates into a 1D model, which can be an arbitrarily shaped line, Fig. 3.
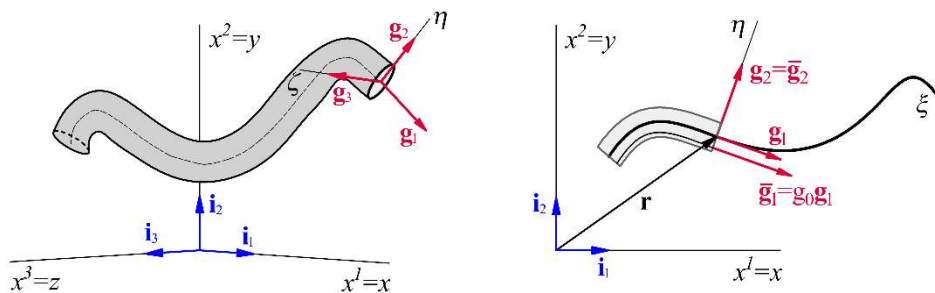

Figure 3. Degeneration of an arbitrarily curved planar beam from 3D to 1D. Coordinate axes and base vectors.

The convective frame of reference (ξ, η, ς) with its base vectors ($\mathbf{g}_1, \mathbf{g}_2, \mathbf{g}_3$) is attached to the beam. The curvilinear coordinate axis ξ coincides with the beam axis while η and ζ are aligned with the principal axes of the second moment of area of the cross section. Due to the BE hypothesis, ξ is the only independent variable in the present analysis [10].

In this section, the lowercase and uppercase boldface letters are used for vectors and second-order tensors, respectively. An overbar designates quantities at the equidistant line of the beam, and the asterisk sign denotes the deformed configuration.

3.2. METRIC OF THE PLANAR BERNOULLI-EULER BEAM

In this paper, only planar beams are analyzed. The position vector of the beam axis is defined with the Cartesian coordinates, $\mathbf{r} = x^\alpha \mathbf{i}_\alpha$, where $\mathbf{i}^\alpha = \mathbf{i}_\alpha$ are the base vectors of the Cartesian coordinate system, see Fig. 3. The tangent base vector $\mathbf{g}_1$ of the beam axis, with respect to the parametric coordinate ξ, is

$$\mathbf{g}_1 = \mathbf{r}_{,1} = \frac{d\mathbf{r}}{d\xi} = x^\alpha_{,1} \mathbf{i}_\alpha, \quad \alpha = 1, 2, \tag{10}$$

while the unit tangent vector follows from the differentiation of the position vector with respect to the arc-length coordinate $\mathbf{r}_{,s} = \mathbf{t}$. The second base vector, $\mathbf{g}_2$, is defined by the rotation of the unit tangent in the counterclockwise direction [11]

$$\mathbf{g}_2 = \Lambda \mathbf{t}, \quad \Lambda = \begin{bmatrix} 0 & 1 \\ -1 & 0 \end{bmatrix}. \tag{11}$$

Now, the metric tensor of a centerline follows as

$$g_{\alpha\beta} = \begin{bmatrix} g_{11} & 0 \\ 0 & 1 \end{bmatrix}, \quad g_{11} = \mathbf{g}_1 \cdot \mathbf{g}_1 = \det\left(g_{\alpha\beta}\right) = g. \tag{12}$$

For an *equidistant line,* which is a set of points with $\eta = const$, the position and the tangent base vectors are

$$\begin{aligned} \bar{\mathbf{r}} &= \mathbf{r}(\xi) + \eta\,\mathbf{g}_2, \\ \bar{\mathbf{g}}_1 &= \bar{\mathbf{r}}_{,1} = \mathbf{g}_1 - \eta K\,\mathbf{g}_1 = g_0\,\mathbf{g}_1, \quad g_0 = 1 - \eta K, \end{aligned} \tag{13}$$

where K is the so-called *signed curvature* measured with respect to the Frenet-Serret frame of reference [10]. The other base vector of the equidistant line is the same as that of the beam axis, $\bar{\mathbf{g}}_2 = \mathbf{g}_2$, and the metric tensor of the equidistant line is

$$\bar{g}_{\alpha\beta} = \begin{bmatrix} g_0^2 g & 0 \\ 0 & 1 \end{bmatrix}, \quad \det\left(\bar{g}_{\alpha\beta}\right) = g_0^2 g = \bar{g}. \tag{14}$$

3.3. KINEMATICS

The deformed configuration of the beam axis is defined by adding the displacement vector of the beam axis $\mathbf{u} = u^{\alpha}\mathbf{i}_{\alpha}$ to the beam axis at the reference configuration, $\mathbf{r}^* = \mathbf{r} + \mathbf{u}$. According to this, expressions (11) and (13) are valid for all configurations.

The displacement vector of an arbitrary point is defined as

$$\bar{\mathbf{u}} = \bar{\mathbf{r}}^* - \bar{\mathbf{r}} = \mathbf{u} + \eta \mathbf{u}_{,2}, \quad \mathbf{u}_{,2} = \mathbf{g}_2^* - \mathbf{g}_2 = \Lambda(\mathbf{t}^* - \mathbf{t}). \tag{15}$$

To define the variation of the kinetic energy, it is necessary to define the acceleration of the beam continuum. First, let us define the velocity of the beam as the material time derivative of displacement [12]

$$\dot{\bar{\mathbf{u}}} = \bar{\mathbf{v}} = \dot{\mathbf{u}} + \eta \dot{\mathbf{u}}_{,2} = \mathbf{v} + \eta \mathbf{v}_{,2}, \quad \dot{\mathbf{u}}_{,2} = \mathbf{v}_{,2} = \dot{\mathbf{g}}_2^*. \tag{16}$$

The velocity of the basis vector $\mathbf{g}_2$ is defined as

$$\mathbf{v}_{,2} = \Lambda \dot{\mathbf{t}}^* = \Lambda \frac{1}{\sqrt{g^*}}(\mathbf{I} - \mathbf{t}^* \otimes \mathbf{t}^*)\mathbf{v}_{,1} = -\frac{1}{g^*}(\mathbf{v}_{,1} \cdot \mathbf{g}_2^*)\mathbf{g}_1^*. \tag{17}$$

This expression can also be found from the Bernoulli-Euler condition of the zero shear strain rate [13]. The angular velocity of the planar BE beam cross section is [12]

$$\omega = \omega^3 = \frac{1}{\sqrt{g^*}}\mathbf{g}_2^* \mathbf{v}_{,1}, \tag{18}$$

which allows us to write Eq. (17) as

$$\mathbf{v}_{,2} = -\frac{1}{g^*}(\mathbf{v}_1 \cdot \mathbf{g}_2^*)\,\mathbf{g}_1^* = -\omega \mathbf{t}^*. \tag{19}$$

The previous relation shows that the velocity of $\mathbf{g}_2$ basis has the direction of the current tangent while its magnitude equals the angular velocity of cross section.

The acceleration of an arbitrary point is obtained as

$$\ddot{\overline{\mathbf{u}}} = \overline{\mathbf{a}} = \dot{\mathbf{v}} + \eta \dot{\mathbf{v}}_{,2}, \tag{20}$$

where

$$\dot{\mathbf{v}}_{,2} = \ddot{\mathbf{g}}_2^* = \frac{3}{g^*}\left(\mathbf{v}_{,1} \cdot \mathbf{t}^*\right)\left(\mathbf{v}_{,1} \cdot \mathbf{g}_2^*\right)\mathbf{t}^* - \frac{1}{\sqrt{g^*}}\left(\mathbf{a}_{,1} \cdot \mathbf{g}_2^*\right)\mathbf{t}^* - \frac{1}{g^*}\left(\mathbf{v}_{,1} \cdot \mathbf{g}_2^*\right)\mathbf{v}_{,1}. \tag{21}$$

Finally, for the variation of both strain and kinetic energy, the virtual displacement of an arbitrary point needs to be defined, i.e.

$$\delta\overline{\mathbf{u}} = \delta\mathbf{u} + \eta\delta\mathbf{u}_{,2}, \quad \delta\mathbf{u}_{,2} = -\frac{1}{\sqrt{g^*}}(\mathbf{t} \otimes \mathbf{g}_2^*)\delta\mathbf{u}_{,1}. \tag{22}$$

3.4. STRESS AND STRAIN

The only non-zero Green-Lagrange component of strain in the BE theory is the axial strain along the tangential direction [13]

$$\overline{\varepsilon}_{11} = g_0\left[\left(1-\eta K\right)\varepsilon_{11} + \eta\kappa\right] + \eta^2\chi\left(\frac{1}{2}\kappa - K\varepsilon_{11}\right), \tag{23}$$

where ε_{11} is the axial strain of the beam axis

$$\varepsilon_{11} = \frac{1}{2}\left(g_{11}^* - g_{11}\right), \tag{24}$$

while κ and χ are the changes of bending curvatures of the beam axis with respect to the parametric and arc-length convective coordinates [14]

$$\kappa = K^* g_{11}^* - K g_{11}, \quad \chi = K^* - K. \tag{25}$$

Considering hyperelastic St. Venant-Kirchhoff material, the only non-zero stress component of the 2nd Piola-Kirchhoff stress is

$$\overline{S}^{11} = E\left(\overline{g}^{11}\right)^2 \overline{\varepsilon}_{11}, \tag{26}$$

where E is the Young's modulus of elasticity and $\overline{g}^{11} = 1/\overline{g}$ is the determinant of the contravariant metric tensor at an arbitrary point.

3.5. VARIATION OF THE STRAIN AND KINETIC ENERGY

The variation of the kinetic energy is

$$\delta\Pi_{kin} = \int_V \rho\overline{\mathbf{a}}\,\delta\overline{\mathbf{u}}\,dV, \tag{27}$$

where

$$\overline{\mathbf{a}} \cdot \delta\overline{\mathbf{u}} = \mathbf{a} \cdot \delta\mathbf{u} + \eta^2\mathbf{P}, \tag{28}$$

and

$$\mathbf{P} = -\frac{2}{g^* g^*}(\mathbf{v}_{,1} \cdot \mathbf{g}_1^*)(\mathbf{v}_{,1} \cdot \mathbf{g}_2^*)(\delta\mathbf{u}_{,1} \cdot \mathbf{g}_2^*) + \frac{1}{g^*}(\mathbf{a}_{,1} \cdot \mathbf{g}_2^*)(\delta\mathbf{u}_{,1} \cdot \mathbf{g}_2^*). \tag{29}$$

The variation of the strain energy is

$$\delta\Pi_{int} = \int_V \overline{S}^{11}\delta\overline{\varepsilon}_{11}\,dV, \tag{30}$$

where the variation of the equidistant strain can be found in [13].
With equations (4), (9), (27), and (30) at hand, it is straightforward to find the spatially discretized equilibrium equation (1). This step is skipped here for brevity.

3.6. TIME DISCRETIZATION

For the time discretization of the spatially discretized equilibrium equation, the well-known HHT-α method is employed. The method is a generalization of the Newmark-β method and it is commonly used in structural dynamics. The equilibrium equation is modified with parameter α that introduces a numerical lag in the internal, external, and contact forces. Basic equations are given in this section while more details can be found in [15].

We are considering the implicit approach where the equilibrium equation is defined at the current, unknown, configuration ($n+1$). The velocity at this configuration is assumed as a sum of the velocity at the previous time increment and acceleration at some point, scaled with the time step

$$\dot{u}_{n+1} = \dot{u}_n + \ddot{u}_\gamma \Delta t. \tag{31}$$

Here, the acceleration at some point is a function of the parameter γ

$$\ddot{u}_\gamma = (1-\gamma)\ddot{u}_n + \gamma \ddot{u}_{n+1}, \quad 0 \le \gamma \le 1. \tag{32}$$

Now, the displacement at the current configuration can be represented as

$$u_{n+1} = u_n + \Delta t \dot{u}_n + \frac{1}{2}\Delta t^2 \ddot{u}_\beta, \tag{33}$$

where the acceleration is assumed as a function of the parameter β, see Eq. (34)

$$\ddot{u}_\beta = (1-2\beta)\ddot{u}_n + 2\beta \ddot{u}_{n+1}, \quad 0 \le 2\beta \le 1. \tag{34}$$

From the previous two equations, it follows that the acceleration at the current configuration can be expressed as

$$\ddot{u}_{n+1} = \frac{1}{\Delta t^2 \beta}(u_{n+1} - u_n) - \frac{1}{\Delta t \beta}\dot{u}_n - \frac{1-2\beta}{2\beta}\ddot{u}_n. \tag{35}$$

The discretized equilibrium equation for one degree of freedom can be written as

$$
\begin{aligned}
&u_{n+1} = u_n + \Delta t \dot{u}_n + \frac{1}{2}\Delta t^2[(1-2\beta)\ddot{u}_n + 2\beta \ddot{u}_{n+1}], \\
&\dot{u}_{n+1} = \dot{u}_n + \Delta t(1-\gamma)\ddot{u}_n + \Delta t \gamma \ddot{u}_{n+1}, \\
&m\ddot{u}_{n+1} + (1+\alpha)(f_{n+1}^{int} - f_{n+1}^{ext} + f_{n+1}^{con}) - \alpha(f_n^{int} - f_n^{ext} + f_n^{con}) = 0.
\end{aligned}
\tag{36}
$$

where m is the mass, f^{int} is the internal force, f^{ext} is the external force and f^{con} is the contact force. The parameter α introduces numerical damping into the system and it is related to parameters β and γ as

$$\frac{-1}{3} \le \alpha \le 0, \quad \beta = \frac{(1-\alpha)^2}{4}, \quad \gamma = \frac{1}{2} - \alpha. \tag{37}$$

The equation (36) is nonlinear and it can be solved using the Newton-Raphson method.

4. NON-UNIFORM RATIONAL B-SPLINES

The non-uniform rational B-splines (NURBS) are the standard tool for geometry modeling in computer-aided design and computer graphics. The aim of this section is to present a brief overview of definitions and properties of the NURBS-based IGA. For a more in-depth discussion on this topic, refer to [16].

A B-spline curve is defined as

$$\mathbf{r}(\xi) = \sum_{i=1}^{n} B_{i,p}(\xi)\mathbf{P}_i, \tag{38}$$

where $\mathbf{P}_i$ are the control points and $B_{i,p}$ are the pth order B-spline basis functions. With a given knot vector $\boldsymbol{\xi} = \{\xi_1, \xi_2, ..., \xi_{N+p+1}\}$, the basis functions can be defined recursively by using the Cox-de Boor formula

$$B_{i,p}(\xi) = \frac{\xi - \xi_i}{\xi_{i+p} - \xi_i} B_{i,p-1}(\xi) + \frac{\xi_{i+p+1} - \xi}{\xi_{i+p+1} - \xi_{i+1}} B_{i+1,p-1}(\xi), \quad B_{i,0}(\xi) = \begin{cases} 1 & \text{if } \xi_i \leq \xi < \xi_{i+1} \\ 0 & \text{otherwise} \end{cases}. \quad (39)$$

Fig. 4 shows an example of the cubic B-spline curve and its corresponding basis functions.
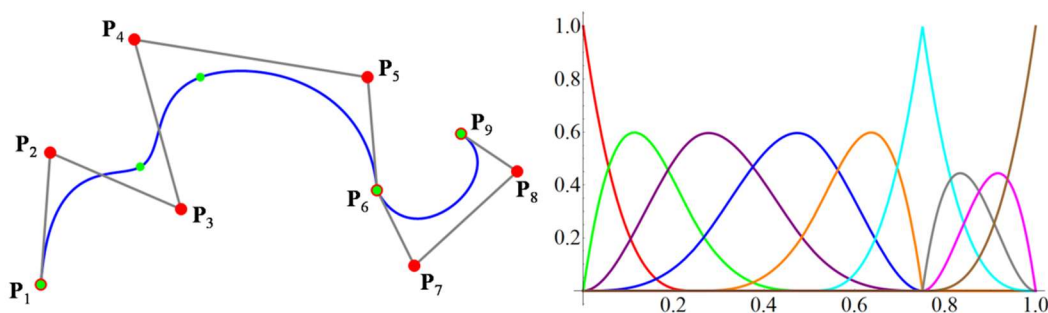
Figure 4. Cubic B-spline curve and corresponding basis functions defined with knot vector
$$\boldsymbol{\xi} = \{0, 0, 0, 0, 0.25, 0.5, 0.75, 0.75, 0.75, 1, 1, 1, 1\}.$$

The curve is interpolatory, and the control polygon is tangent to the curve at the both first and last control points, due to the fact that the knot vector is open. Additionally, the curve is also interpolatory at the control point $\mathbf{P}_6$, because the multiplicity of the knot $\xi = 0.75$ is equal to the polynomial order $p = 3$. The B-spline basis functions constitute a partition of unity, they are non-negative for any value of parameter ξ, and they are C^{p-m} continuous at knots of multiplicity m. The more general NURBS is defined as

$$\mathbf{r}(\xi) = \sum_{i=1}^{N} B_{i,p}(\xi) w_i \mathbf{P}_i \Big/ \sum_{j=1}^{N} B_{j,p}(\xi) w_j = \sum_{i=1}^{N} R_{i,p}(\xi) \mathbf{P}_i, \quad (40)$$

where w_i are the weights and $R_{i,p}$ are the rational basis functions. The rational basis functions have the same main properties like the B-spline basis. The NURBS curve becomes B-spline when all weights are equal.

The main idea of IGA is to use these NURBS functions for both the initial geometry and unknown fields. This results in a higher-order accurate spatially discretized model that is applicable in various fields of computational mechanics [5].

5. NUMERICAL EXPERIMENT

To test the CG and IPIP approaches in the contact dynamics, an example of the impact and multiple collisions of two beams is considered in this section. The problem setup is given in Fig. 5. The upper beam falls due to gravity and hits the lower beam. After the initial impact, both beams start to oscillate, and a range of further collisions occur. No physical damping is introduced into the system, and the complete dissipation of the energy is due to the numerical damping. For the comparison of different approaches, the deflection of the point A is followed. We will first consider the results obtained with the adopted numerical models, and then discuss the effects of some input parameters.
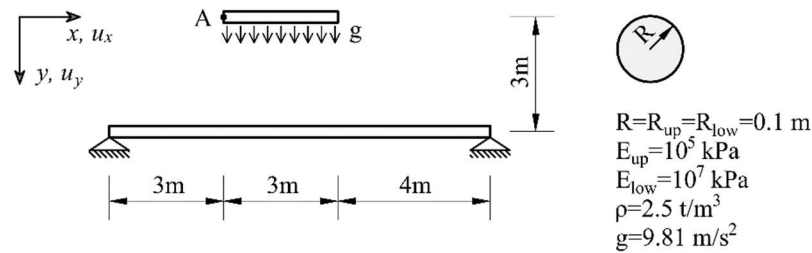
Figure 5. Free fall of an elastic beam onto another beam. Problem setup.

The simulation snapshots obtained with the adopted CG model are shown in Fig. 6. The complicated dynamical behavior with multiple collisions is evident. The results obtained with the adopted CG, IPIP, and Abaqus models are presented in Fig. 7. All three computational models give different results, but the general behavior is similar. The process starts with the free fall of the upper beam and continues with the first impact at $t = 0.75\,s$. Due to this impact, the lower beam accelerates, deflects, and separates from the upper beam, which slows down and continues its free fall until the next collision. The point of the first impact is the same for all models, but the point of the second collision differs. This collision occurs when the lower beam rises, impacts the upper beam, and launches it upwards. As a result, we can observe the first amplitude that is similar for all models ($\approx -2.25\,m$) but occurs in different instances. The process continues with subsequent falls, oscillations, and collisions.
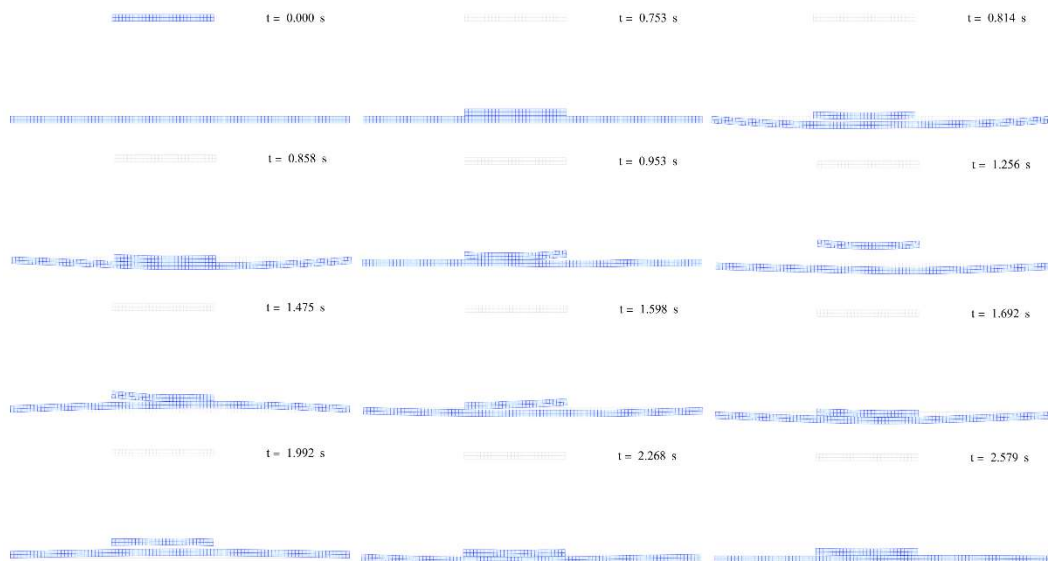

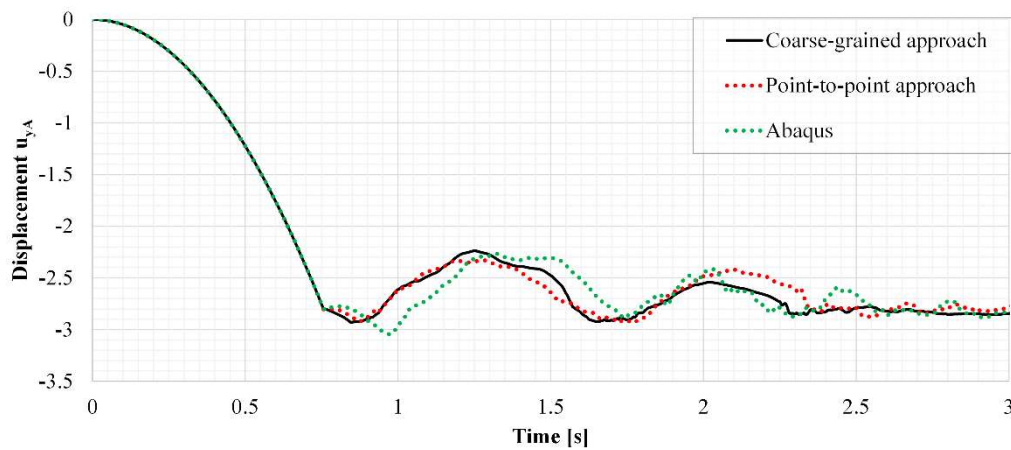*Figure 6. Simulation snapshots. Animation is available as supplementary data at [17].*

Figure 7. Comparison of the deflection of point A. Adopted models: Abaqus vs. CG approach vs. IPIP approach.

Next, let us discuss some details of the adopted models. The CG and IPIP models are discretized with 20 elements for the lower, and 6 elements for the upper beam. Quartic B-spline basis functions with C^1 continuity are employed. For the integration of the contact energy term Π_{con}, each element is divided into 20 segments with one integration point per segment. The integration of the internal and inertial contributions is made with 5 integration points per element.

The simulation results obtained with the IPIP approach are very sensitive with respect to the penalty parameter ε, see Fig. 8. The first displacement amplitude after the initial impact increases with the decrease of the parameter ε. For the comparison of different models in Fig. 7, the value of 10^6 is adopted since it fits best the other approaches. Regarding the numerical damping, the effect of the α parameter is considered in Fig. 9 for the IPIP model. As expected, smaller values of the parameter α provide an additional numerical damping. This is evident from the comparison of the first amplitudes. However, after this amplitude, it is difficult to make a clear conclusion about the energy dissipation due to the multiple collisions. The value that provides the highest numerical damping is adopted, $\alpha = -0.33$.
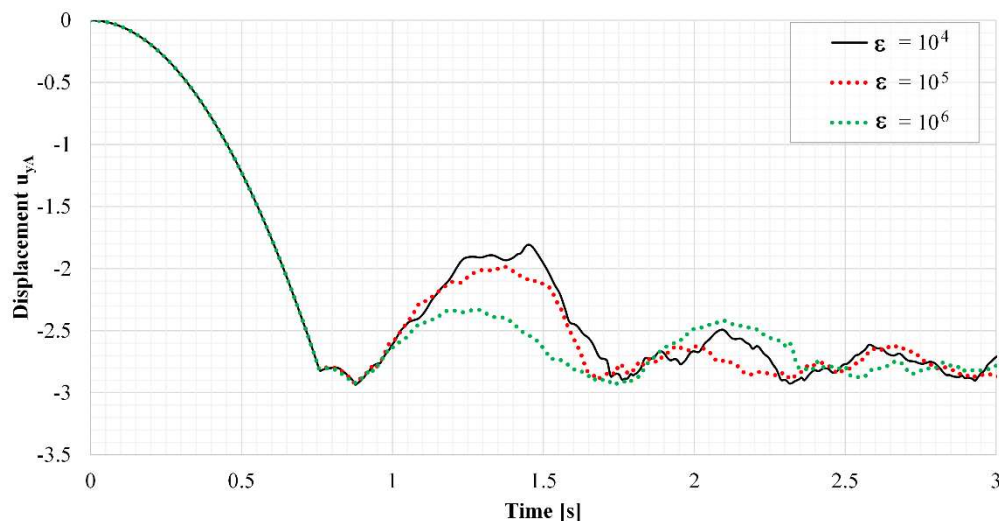

Figure 8. Comparison of the deflection of point A. IPIP approach: influence of the penalty parameter.
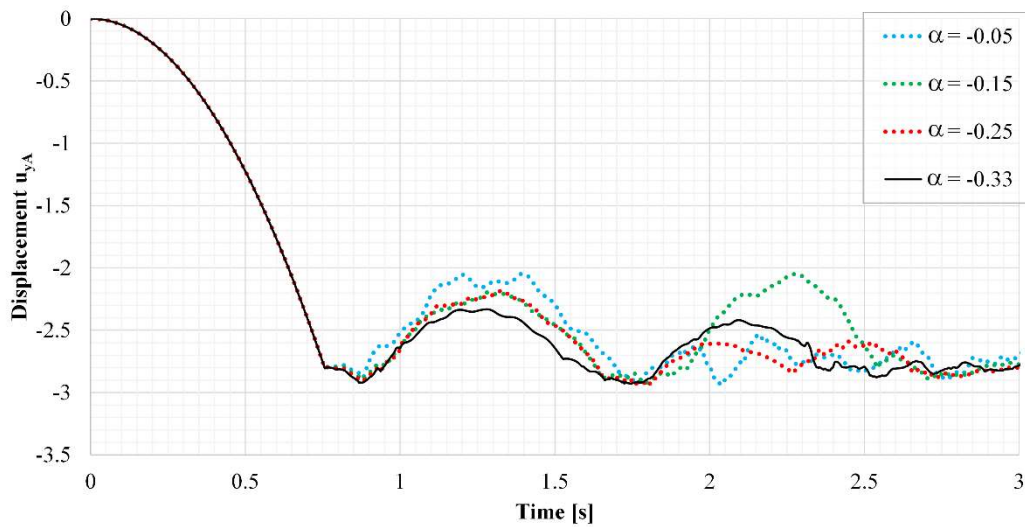
Figure 9. Comparison of the deflection of point A. IPIP approach: influence of the parameter alpha.

Regarding the CG approach, the contact is modeled with steric interaction potential, $m = 12$. Particle densities are set as $\beta_1 = \beta_2 = 1$ while the material constant is $k_m = 5 \cdot 10^{-25}$. The effect of the cutoff distance on the CG simulations is investigated and the results are given in Fig. 10. The cutoff distance does not have a significant influence on the first amplitude, but its effect increases as the simulation develops further. For the comparison in Fig. 7, the cutoff distance of 0.3 is adopted in our CG model.
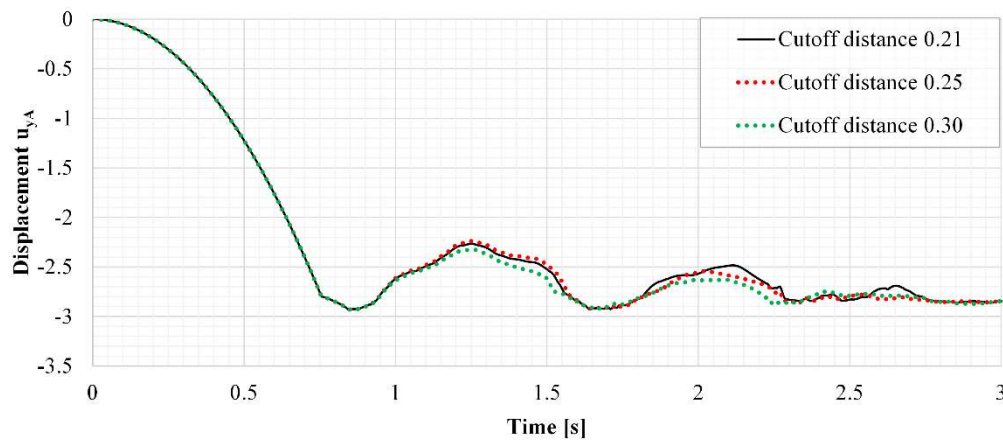

Figure 10. Comparison of the deflection of point A. CG approach: influence of the cutoff distance.

The Abaqus model is discretized with 28304 solid C3D8R elements (8-node linear brick, reduced integration, hourglass control) [18]. Our initial model was based on beam elements, but an issue with unphysical penetration between beams occurred. Therefore, we have utilized the 3D solid model with a restrained displacement component perpendicular to the beams' plane. Explicit analysis and general contact are selected as a contact dynamics procedure, while the normal contact property and the bulk viscosity parameters are varied. The bulk viscosity introduces numerical damping into the system. The results obtained with three combinations of the bulk viscosity parameters are shown in Fig. 11. We can observe that the quadratic parameter practically does not influence the response during the first 2 seconds. The default values of the linear/quadratic bulk viscosity parameters are adopted, i.e. 0.06/1.2. Regarding the normal contact property, we have considered two overclosure-contact pressure relations: the *hard* contact model and the linear contact model. The tangential part of the contact is modeled as frictionless. The comparison of models with different normal contact properties is shown in Fig. 12 where the values of contact stiffness for the

linear contact model are varied. With the increase of the stiffness parameter, the results of the linear model approach those of the *hard* contact model. Significant changes in the simulated contact dynamics problem due to relatively small changes in the contact properties are observed. For the comparison of approaches, we have adopted the model with the linear overclosure-contact pressure relation and the contact stiffness of 10^7.
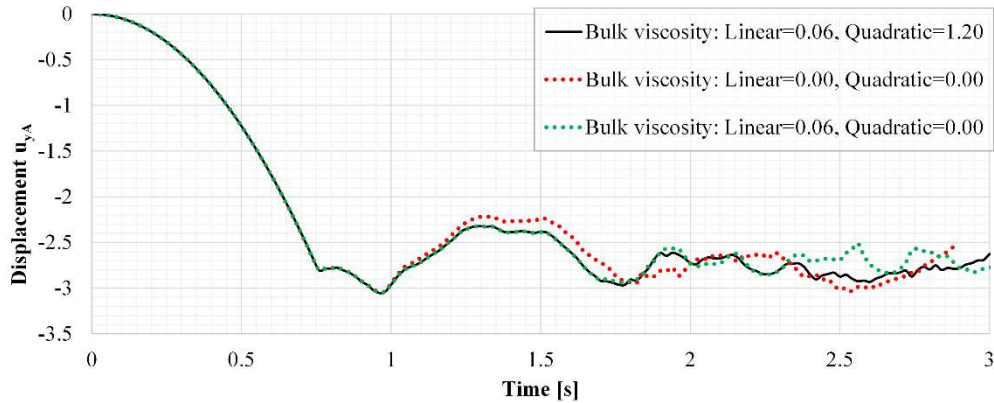

Figure 11. Comparison of the deflection of point A. Abaqus: influence of the bulk viscosity parameters.
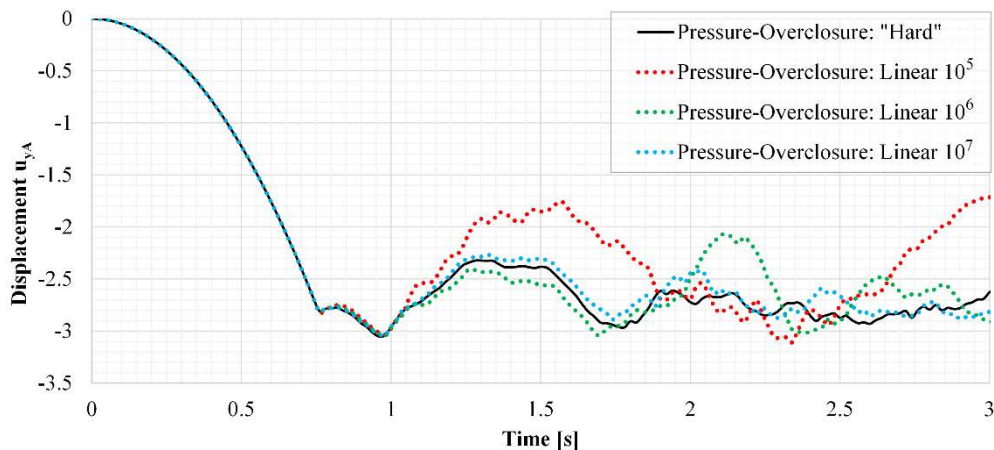

Figure 12. Comparison of the deflection of point A. Abaqus: influence of the overclosure-contact pressure relation.

6. CONCLUSIONS

The contact dynamics between planar beams is considered. Two computational approaches are utilized for contact modeling: the standard continuum approach and the coarse-grained approach. For the continuum approach, we consider the point-to-point contact discretization, while the contact constraint is introduced by the penalty function. The closest point-pairs are found from a set of densely distributed integration points.

The coarse-grained approach uses the section-section interaction potential between circular disks to reduce the underlying integral from 6D to 2D. This formulation is more computationally expensive than the point-to-point approach, but provides a more accurate distribution of contact tractions.

For the adopted example, all utilized approaches are sensitive with respect to a variety of input parameters, such as contact stiffness and numerical damping. Future research should focus on a detailed analysis of spatial beams and include the effects of material and structural damping.

ACKNOWLEDGMENTS

LITERATURE

[1] J. N. Israelachvili, *Intermolecular and Surface Forces*. Academic Press, 2010.

[2] R. A. Sauer and S. Li, "A contact mechanics model for quasi-continua," *Int. J. Numer. Methods Eng.*, vol. 71, no. 8, pp. 931–962, 2007, doi: 10.1002/nme.1970.

[3] P. Wriggers, *Computational Contact Mechanics*, 2nd ed. Springer Berlin, Heidelberg, 2006.

[4] M. J. Grill, W. A. Wall, and C. Meier, "A computational model for molecular interactions between curved slender fibers undergoing large 3D deformations with a focus on electrostatic, van der Waals, and repulsive steric forces," *Int. J. Numer. Methods Eng.*, vol. 121, no. 10, pp. 2285–2330, 2020, doi: 10.1002/nme.6309.

[5] T. J. R. Hughes, J. A. Cottrell, and Y. Bazilevs, "Isogeometric analysis: CAD, finite elements, NURBS, exact geometry and mesh refinement," *Comput. Methods Appl. Mech. Eng.*, vol. 194, no. 39, pp. 4135–4195, 2005, doi: 10.1016/j.cma.2004.10.008.

[6] P. Wriggers and G. Zavarise, "On Contact Between Three-Dimensional Beams Undergoing Large Deflections," *Commun. Numer. Methods Eng.*, vol. 13, no. 6, pp. 429–438, 1997, doi: 10.1002/(SICI)1099-0887(199706)13:6<429::AID-CNM70>3.0.CO;2-X.

[7] C. Meier, W. A. Wall, and A. Popp, "A unified approach for beam-to-beam contact," *Comput. Methods Appl. Mech. Eng.*, vol. 315, pp. 972–1010, 2017, doi: 10.1016/j.cma.2016.11.028.

[8] R. A. Sauer and L. De Lorenzis, "A computational contact formulation based on surface potentials," *Comput. Methods Appl. Mech. Eng.*, vol. 253, pp. 369–395, 2013, doi: 10.1016/j.cma.2012.09.002.

[9] A. Borković, M.H. Gfrerer, R.A. Sauer, B. Marussig, and T.Q. Bui, "A novel section-section potential for short-range interactions between plane beams," Preprint to be published at ArXiv.

[10] A. Borković, S. Kovačević, G. Radenković, S. Milovanović, and M. Guzijan-Dilber, "Rotation-free isogeometric analysis of an arbitrarily curved plane Bernoulli–Euler beam," *Comput. Methods Appl. Mech. Eng.*, vol. 334, pp. 238–267, 2018, doi: 10.1016/j.cma.2018.02.002.

[11] A. Borković, B. Marussig, and G. Radenković, "Geometrically exact static isogeometric analysis of arbitrarily curved plane Bernoulli–Euler beam," *Thin-Walled Struct.*, vol. 170, p. 108539, 2022, doi: 10.1016/j.tws.2021.108539.

[12] G. Radenković, Finite rotation and finite strain isogeometric structural analysis (in Serbian). Belgrade: Faculty of Architecture, 2017.

[13] A. Borković, M. H. Gfrerer, and B. Marussig, "Geometrically exact isogeometric Bernoulli–Euler beam based on the Frenet–Serret frame," *Comput. Methods Appl. Mech. Eng.*, vol. 405, p. 115848, 2023, doi: 10.1016/j.cma.2022.115848.

[14] G. Radenković and A. Borković, "On the analytical approach to the linear analysis of an arbitrarily curved spatial Bernoulli–Euler beam," *Appl. Math. Model.*, vol. 77, pp. 1603–1624, 2020, doi: 10.1016/j.apm.2019.09.012.

[15] H. M. Hilber, T. J. R. Hughes, and R. L. Taylor, "Improved numerical dissipation for time integration algorithms in structural dynamics," *Earthq. Eng. Struct. Dyn.*, vol. 5, no. 3, pp. 283–292, 1977, doi: 10.1002/eqe.4290050306.

[16] L. Piegl and W. Tiller, *The NURBS Book*. in Monographs in Visual Communications. Berlin, Heidelberg: Springer Berlin Heidelberg, 1995. doi: 10.1007/978-3-642-97385-7.

[17] *Free fall of a flexible elastic beam onto another beam*, (Apr. 04, 2024). doi.org/10.3217/51dzd-9yr50.

[18] M. Smith, "ABAQUS/Standard User's Manual, Version 6.9," 2009.